Tuijin Jishu/Journal of Propulsion Technology
ISSN: 1001-4055
Vol. 44 No. 6 (2023)

Excellent Electromagnetic Wave Absorbing Performance of Carbon Nano Structure Synthesized from *Oryza Sativa* Stems

Brijesh Gaud[1], Kshirsagar Dattatray[2], Debdatta Ratna[3], and Sandesh Jaybhaye[4*]

[1,4] *Department of Chemistry, B. K. Birla College, (Autonomous), Kalyan, Maharashtra, India*
[2] *Department of Physics, B. K. Birla College, (Autonomous), Kalyan, Maharashtra, India*
[3] *Naval Materials Research Laboratory, Ambernath, Maharashtra, India*

Abstract:-Currently, electromagnetic threat increased duo to interaction of electromagnetic wave with biological objects as a result of electromagnetic pollution of the environment. This is caused by different sources, like local wireless networking, extensive electronic device in households and public spaces, exhaustive consumption of electromagnetic filed in medicine and biological chemistry, and technologies. electromagnetic pollution not only effect the electronic device but also human organs like heart and biological system hence more attention are paid to develop such materials which are able to absorb electromagnetic wave. The carbon-based nano structure is good candidate because of its excellent dielectric properties high surface area and hence shows better electromagnetic waveabsorbing performance. The synthesis of Carbon Nano Structure obtained from plant-based precursors has become one of the newest approaches in the field of electromagnetic waveabsorbingabsorption due to its economical, immense availability and sustainability.Waste obtained from agriculture i.e., stem of rice crop was used as source of carbon to obtained carbon nano fibers (CNFs) over in inert atmosphere of Hydrogen gas. Acid treated CNFs were characterized using XRD, FEG-SEM, EDAX, and Raman Spectroscopy. The range of diameter and length of CNFs obtained from stem of rice crop are 100-200nm, 100-800nm, respectively. CNFs/epoxy composite with 9 wt. % and 2.4 mm thickness, shows an optimal Reflection loss (RL) value of -13.75 dB at 9.78 GHz. The effective absorption (RL ≤ -10 dB) has a bandwidth 8.41-11.88 GHz.

Keywords*:Electromagnetic Threat, Electromagnetic Pollution, Absorbing Material, Stem of Rice Crop and CNFs/epoxy Composite*

1. Introduction

The utilization of microwave absorbing materials (MAMs) started during the Second World War 1930's soon next the innovation of radar. Nowadays, applications of Frequency Selective Surfaces (FSS) for radar-absorbing materials (RAM) or MAMs**.**MAMs can reduce the detectability of satellites and aircraft, which can protect targets from directed energy weapons, is alleviated, to some extent during war [1, 2]. The fast-growing electronic and communication devices for the commercial and defense industry and the use of GHz frequency, lead to increasing of electromagnetic radiation pollution worldwide. The electromagnetic threat heightened duo to contact of electromagnetic wave with biological objects as a result of electromagnetic pollution of the environment[3]. In order to eliminate electromagnetic interference and electromagnetic radiation pollution the development of high-performance electromagnetic wave-absorbing materials with a wide range of frequencies, strong absorption, and tunable electromagnetic properties have been comprehensively investigated by researchers. MAMs are presently paid more consideration.

Traditional MAMs consists of ferrites and magnetic metals such as Fe_3O_4[4], SiC[5], $BaTiO_3$[6], magnetic metal powders and related ferrites *etc.* for excellent microwave absorption properties, but due to high density and poor corrosion resistance limit the sustainable progress as MAMs. Carbon based nanostructure like fullerene, Carbon nano tubes (CNTs), Carbon nano fibers (CNFs) and Graphene have attracted researcher worldwide and are

studied comprehensively duo to its outstanding physio-chemical properties [7]. Conventionally the, the precursors used in the synthesis of carbon nano materials are fossil fuels and petroleum products such as methane, benzene, xylene, toluene, etc. The availability of such precursor and its cost are factors that affect the cost of finally produced carbon nanomaterial [8, 9]. Hence, there is a need to search for new sources of precursors, which are not fossil-fuel based.Plant based precursors as source of hydrocarbons for synthesis of Carbon nanomaterial's, are leading inspiration due to widely available in nature, renewable, cheap and have the potential to be the greener approach for large scale production of carbon nano materials.

As per the principal of green chemistry, the raw materials of any chemical process must be renewable and harmful of natural nature. Additionally, the synthesis method designed in such a way that the maximum raw materials was converted into the product. The use of plant-based precursor and waste natural product for synthesis of multifunctional carbon nano materials are follows the above two principles of green chemistry hence it attracted more consideration as an environmentally friendly, safe and cheapest methods for the synthesis of carbon nano materials. Recent reports have revealed that the porous structure of carbon nano materials is beneficial for enhancing microwave absorption. The leading inspiration of using non fossil sources is to provide greener and inexpensive raw materials for large-scale making of carbon-based nano structures. Plant based precursors have the potential to address the above problems.

2. Materials and Methods

2.1. Materials

CNFs were synthesized from organic waste precursor i.e., *Oryza Sativa* Stems collected fromwere collected from Kalyan market (near to college campus). Rice is the most important food crop of the developing world and the staple food of more than half of the world's population. Stem of rice grass popularly known as the haulm or the culm (generally erect, cylindrical, and hollow) are use as carbon source for synthesis of CNFs [10, 11]. High purity of Hydrogen gas was provided by gas-world corporation Ulhasnagar, Kalyan. The chemical reagents used for the experiment were have analytically grade purity, and were used without further purification. The distilled water used in the experiment was double distilled water collected from in our lab.

2.2. Methods

The conventional methods for the synthesis of CNFs are slow and energy intensive because of that they contribute the high cost for production. The high cost of production limits the application. Alternative methods have been investigated over the years with advanced manufacturing technologies and alternative precursors (carbon source) such as bio-mass or agriculture waste help to reduce, CNFs cost and dependence on fossil feedstock. This research work was focused on biomass-based precursors, which used for synthesis of CNFs. The steps involved in synthesis of CNFs using biomass precursor are illustrated in figure 1. The stem of rice crop was washed with distilled water to remove surface contamination like dust, pesticide, etc. It was then soaked in 10% KOH solution for 24 h. The soaked samples were washed with distilled water several times to reach the neutral pH and dried in oven at 120^{o}C. Finally, the dried parts of plant were thermally pyrolysis at 900^{o}C under inert atmosphere of Hydrogen gas for 120 min. in a horizontal furnace. At the end, the furnace is turned off until the reactor cools down to room temperature. CNFs fiber synthesized from stem of rice crop are designated asR-CNFs. Synthesized R-CNFs were treated with 50% Conc. HCl and HNO_3 to remove the alkali, amorphous carbon and metals present. Finally, the R-CNFs were filtered and washed with distilled water several times to reach neutral pH i.e.,7 and dried in an oven at 100^{o}C and powdered [2, 12].

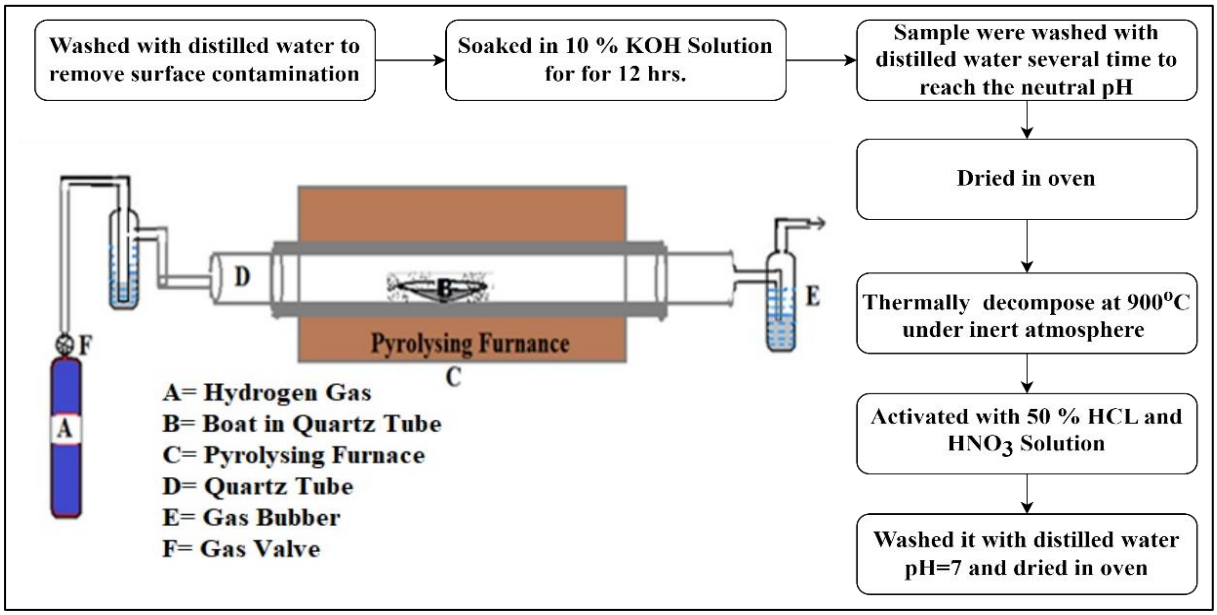

Figure 1 Schematic Diagram for Step Involved and CVD Furnace used in Synthesis of CNFs Using Precursor Derived from Bio-Mass/Plant Passed.

3. Characterization

Purified CNFs powder obtained after pyrolysis were characterized using following analytical instruments:

3.1. Fourier Transform Infrared (FTIR) Spectroscopy

The chemical structure of the samples was examined using a FTIR Spectroscopy Jasco model No. 4100 in a wavenumber range of 400–4000 cm^{-1}set up at B. K. Birla College, Kalyan, India.

3.2. X-ray diffraction (XRD)

XRD patterns were recorded using a D2 phaser second generation X-ray diffractometer (Bruker, Bremmen, Germany) with a Cu Ka radiation (λ = 1.5418 Å) at a scanning speed of 10°/min from 10° to 80°.

3.3. Raman Analysis

Raman spectra were collected using the Laser Raman Spectroscopy HR800-UV confocal micro-Raman spectrometer, Horiba Jobin Yvon, France at SAIF, IIT Bombay in a range of 500–3000 cm^{-1}.

3.4. Thermogravimetric analysis (TGA)

The TGA is performed on a TGA Model: Tecnai G2, F30 at a heating rate of 10 °C/min under a nitrogen atmosphere with a flow rate of 50 mL/min at NMRL, DRDO, Ambarnath, India.

3.5. Surface Area Analysis (BET Analysis)

Surface area were analysed by nitrogen adsorption analyses implemented on single port Brunauer–Emmett–Teller (BET) analyzer (smart instrument, dombiwali, India).

3.6. Field Electron Gun -Scanning Electron Microscope (FEG-SEM)

The morphology of all samples was visualized by a FEG-SEM model of JSM—5410, courtesy of JEOL, USA at SAIF, IIT Bombay with an accelerate voltage of 30 kV.

3.7. High Resolution -Transmission Electron Microscopy (HR-TEM300)

The morphology of all samples was visualized by the HR-TEM of 300Kv Model: Tecnai G2, F30 at SAIF, IIT Bombay.

3.8. Microwave Absorption study of CNF/ epoxy composites

The complex permittivity and permeability of the samples were measured using a vector network analyzer (VNA) (Model; N5227B, 10 MHz to 67 GHz, Key sight Technologies, USA) in the frequency range of 8.2-12.4 GHz by transmission/reflection wave guide method. Full two port calibration of the measurement setup was carried out prior to the measurements to remove the errors due to load match, source match, directivity, isolation etc. Rectangular shape samples having dimensions of length (22.86 mm) width (10.16 mm) were cut as per the WR 90 wave guide size sample holder. Complex relative permittivity and permeability were determined from the measured scattering parameter using Key sight software module N1500A [13].

4. Results and Discussion

Stem of Rice Crop naturally features hollow microstructures with good porous structure that are favour the improving impedance matching and attenuation capacity[14–16] . The Oven-dried Stem of Rice Crop was carbonized at 900 °C for 120 min. under a Hydrogen atmosphere to obtain the R-CNFs.To gain more insight into the variation of the nanostructure after carbonization, FT-IR, TGA and XRD, SEM and TEM of the post-carbonized cylindrical samples were performed and the results are represented as follows:

3.9. FT-IR Analysis

The FT-IR spectra of R-CNFs synthesized by stem of rice crop were shown in figure 2. It is seen that the band observed to various cellulose molecules with induced characteristic peaks at 3431, 2936, 1595, 1397, 1114, 1063, 708 and 622 cm^{-1}. Utmost such bands have been also reported by other researchers for different kind of CNFs [17].The band at around 3431 cm^{-1} are assigned to the –OH vibrational stretching mode of hydroxyl functional group. The band at around 2936 cm^{-1} are assigned to the -CH stretching mode. The bands at about 1595 cm^{-1} are the characteristic of the C-O and C≡C stretching. The peaks obvers at 1397cm^{-1} are assign to C-H bending and 1114 and 1063 cm^{-1} are assigned for bending vibration mode of functional group attached to -OH atom like conjugated C-O stretching, C-O stretching in carboxylic groups, and carboxylate moieties [18] The band at around 705 cm^{-1} and band at around 622 cm^{-1} are assigned to the C=C bending mode.

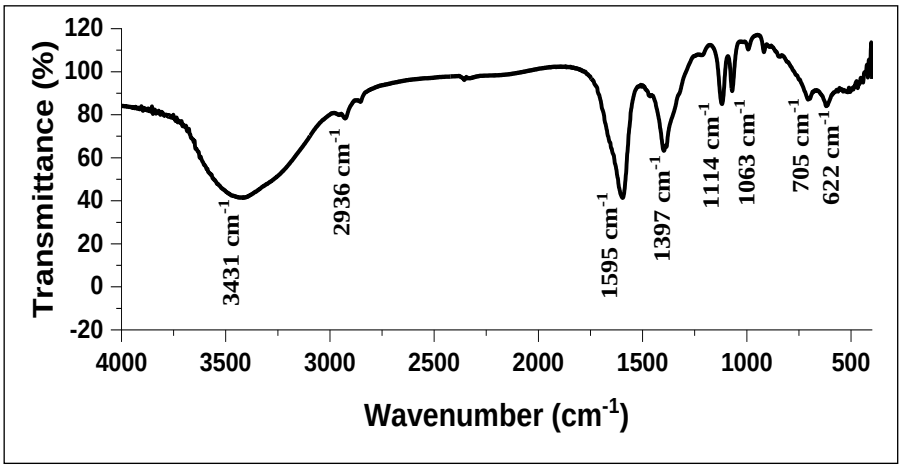

Figure 2. FT-IR Spectrum of R-CNFs Synthesized using Stem of Rice Crop.

3.10. XRD Analysis

The XRD pattern of R-CNFs synthesized by stem of rice crop were shown in figure 3. XRD profiles of the purified R-CNFs shows the diffraction peak at 2θ = 26.46° indexed as [002] reflection for characteristic graphitic carbon according to PDF JCPDS: 00-008-0415. The low intensity peak at 44.41^0 is attributed due to the graphite like structure corresponding to the [100] plane. In addition, the positions and relative intensities of peaks present in figure 3, related with metallic particles at 2θ = 42.35^0 and 54.59^0 indicate the presence of metallic particles in Stem of Rice crop.

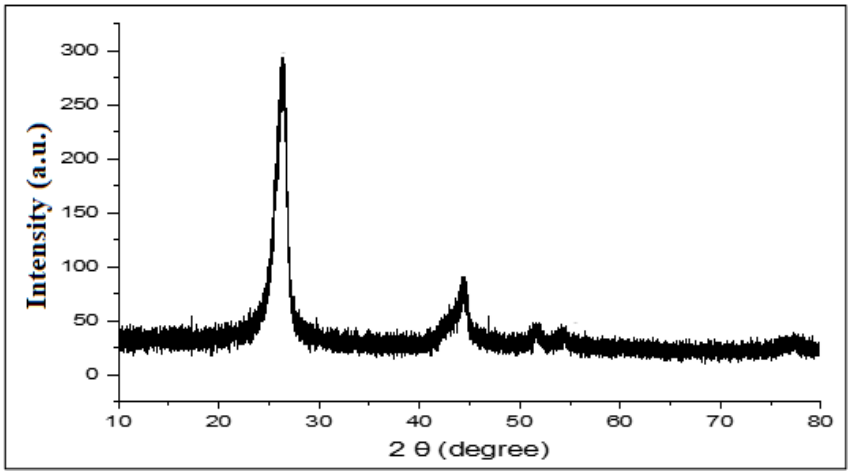

Figure 3. XRD Pattern of R-CNFs Synthesized from Stem of Rice Crop.

3.11. Raman Analysis

The Raman spectra of R-CNFs synthesized by stem of rice crop were shown in figure 4. Spectrum profiles of the purified R-CNFs shows two separate peaks at 1348 and 1583 cm^{-1}[19, 20]. Which correspond to D and G Band respectively. The intensity ratio of the D band to the G band (I_D/I_G) is often used to estimate the defect concentration in carbon materials. The low value of I_D/I_G ratio indicates high graphitization and high value of I_D/I_G ratio is usually ascribed to the presence of defects on R-CNFs. The I_D/I_G ratio of R-CNFs is 0.58 indicates a high graphitization[21]. The D mode which corresponds to sp^2 hybridized carbon and G band is due to the C–C stretching in the graphitic material. The second order D-band (also called the 2D-band), peaks at 2785 cm^{-1} are due to asymmetrical C–H stretching vibrations of the CH_2 group [22].

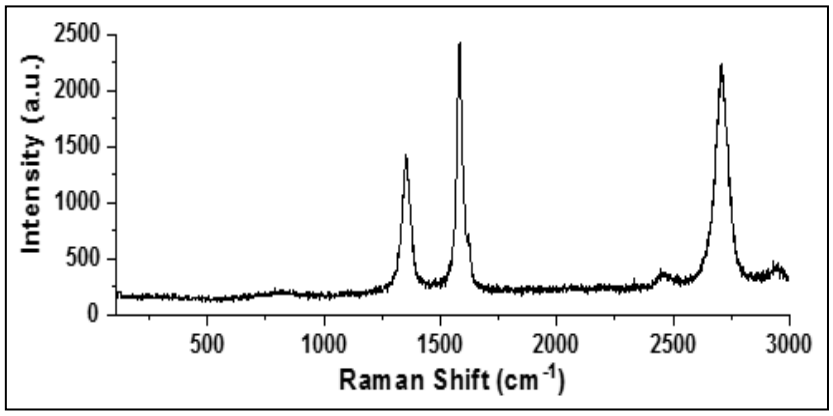

Figure 4. Raman Spectra of R-CNFs Synthesized from Stem of Rice Crop

3.12. SEM Analysis

The SEM image of R-CNFs synthesized using stem of rice crop and the tube diameters and tube length size distribution of R-CNFs using SEM image, processing using the ImageJ software are shown infigure 5. (a), (b) and (c) respectively. SEM analysis shows that the tube diameter and length of theR-CNFs are in the range of 100-280 nm and 100-800 nm respectively. The average tube diameter and length of the R-CNFs are 161 nm and 587 nm respectively. SEM image of the purified R-CNFs revealed that CNFs are tubular and having porous structure. SEM image also shows that on the outer diameter of R-CNFs are 73.2 nm and inner diameter was 35.8 nm.

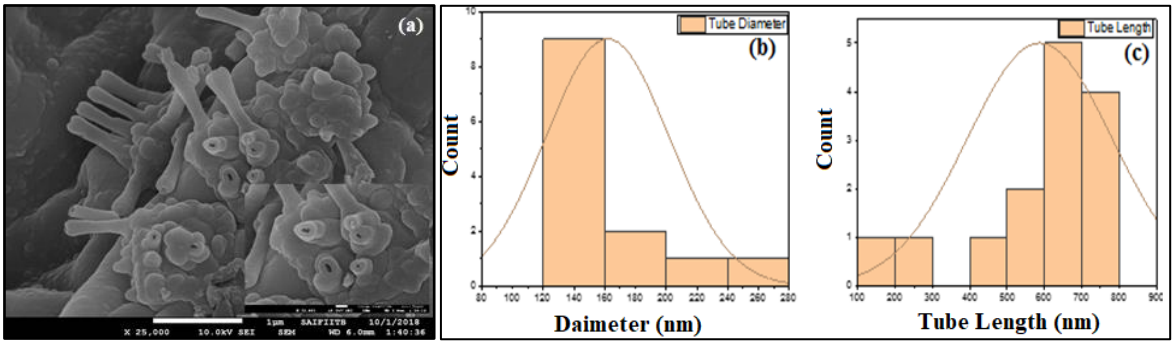

Figure 5. (a) SEM Image and (b) Tube Diameter and (c) Tube Length Distribution Histogram of R-CNFs Synthesized from Stem of Rice Crop.

3.13. EDX Analysis

In order to analyze the elemental components after activation of stem of rice crop, the EDX spectra of were analyzed. The EDX image of R-CNFs synthesized by stem of rice crop were shown in figure 6. The EDX image of the purified R-CNFs indicate that carbon fiber after pyrolysis and activation contained different elements such as Carbon, Oxygen, Calcium, Magnesium and silica. The carbonated stem of Rice crop retained high levels of Oxygen, Calcium, Magnesium and Silica because the raw material itself contained these elements

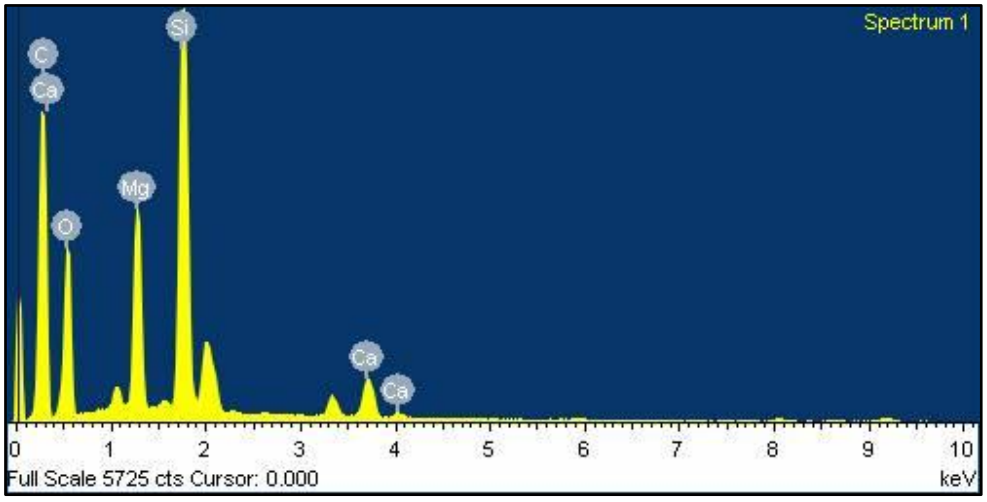

Figure 6. EDX Image of R-CNFs Synthesized from Stem of Rice Crop.

3.14. TEM Analysis

The TEM image of R-CNFs synthesized by stem of rice crop were shown in figure 7. **T**EM images have been used to further observe nano structures of R-CNFs. From figure 7 it is seen that the R-CNFs have bundles of nano fibers in the range of 80-120 nm.

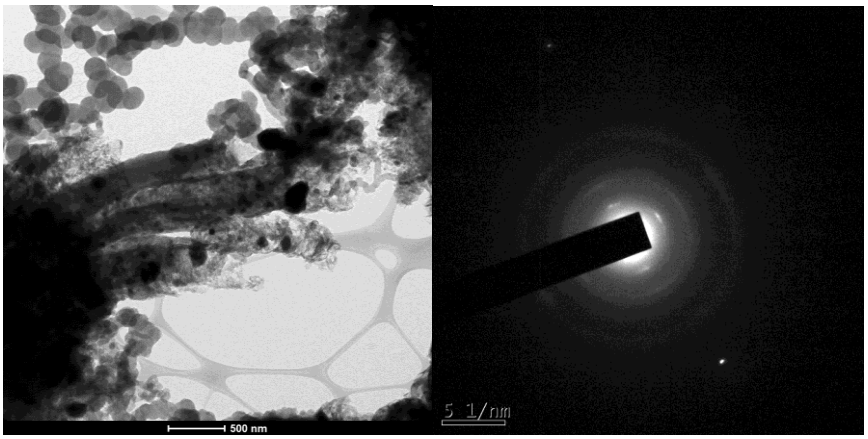

Figure 7.TEM Image of R-CNFs Synthesized from Stem of Rice Crop

3.15. TGA Analysis

Thermo-gravimetric analysis was carried out for investigating the decomposition process and purity of R-CNFs. Sample was heated under the dry Nitrogen flux from room temperature to 800°C with heating rate 10°C min^{-1}.The derivative of the TGA with respect to temperature (dTGA) of the R-CNFs was shown in figure 8 to improve resolution of small changes in mass, characteristic peaks in the dTGA. The peaks were observed at 59, 386, and 731°C. The peak at 59°C is associated with loss of moisture, although the fibers were dried before the analysis, the peak at 386°C is associated with the decomposition of some light weight molecule (cellulose), and after the peak at 731°C only the ashes can be seen.

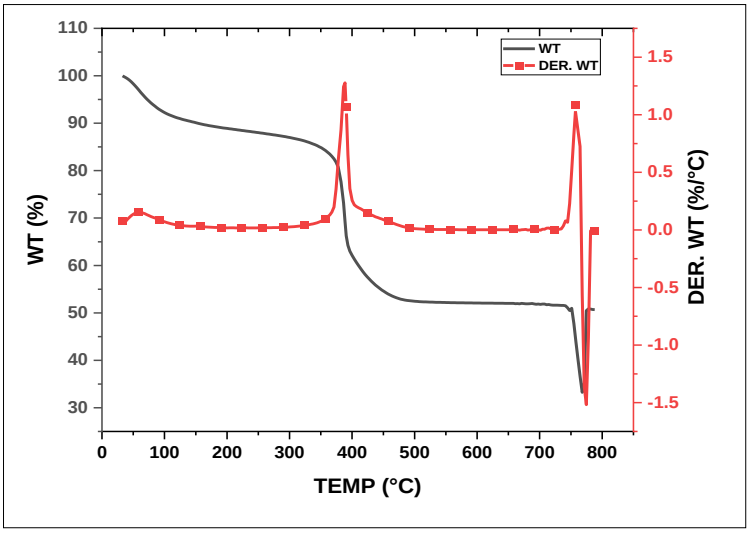

Figure 8. TGA Curve of R-CNFs Synthesized from Stem of Rice Crop

3.16. Microwave-Absorbing Performance

Generally, the microwave-absorbing performance of an MAM is expressed by reflection loss (R_L), and the smaller R_L means less reflected energy. Normally, a R_L value of lower than −10 dB refers more than 90% of penetrated electromagnetic energy can be effectively converted into another form of energy. Correspondingly, the frequency range in which R_L value is smaller than −10 dB is defined as an effective absorption bandwidth [23], representing the frequency window for practical application. For a desired MAM, the R_L should be as low as possible and the absorption bandwidth as wide as possible.

The microwave absorption properties of the materials are related to the fundamental physical quantities: relative complex permittivity (ε) and permeability (μ.). The R_L of MAMs i.e., Epoxycomposite of R-CNFs was measured and calculated with the help of Relative complex permittivity $\epsilon_r = \epsilon' - j\epsilon''$ and permeability $\mu_r =$

$\mu' - \mu''$. As we know that real parts of Relative complex permittivity (ϵ') are known as electric energy storage or the ability of the material to be polarized and permeability (μ') are known as the magnetic energy storage. The imaginary parts of Relative complex permittivity (ϵ'') are represent the loss of electric, where permeability (μ'') represent magnetic energy [24–26].

On the basis of transmission line theory, the R_L of an absorber can be calculated from its EM parameters according to the following formula [27, 28]:

$$Z_{in} = Z_o \sqrt{\frac{\mu_r}{\varepsilon_r}} \tanh\left(\frac{j2\pi f d\sqrt{\mu_r \varepsilon_r}}{c}\right)$$

$$R_L = -20 \log 10 \left|\frac{(Z_{in} - Z_o)}{(Z_{in} + Z_o)}\right|$$

Where,

Z_{in} are the input impedance,

Z_o is free-space impedance,

f is the frequency,

d is the absorber thickness, and

c is the light velocity.

3.17. *Relative complex Permittivity and Permeability of R-CNFs/Epoxy Composite*

Relative complex permittivity and permeability of R-CNFs/Epoxy composite having 2.5 mm thickness was studied for 3, 5, 7 and 9 wt. % of R-CNFs composition. The real and imaginary part of the relative complex permittivity of the R-CNFs/Epoxy composites in the frequency range 8.2 -12.4 GHz (X-Band) are shown in figure 9. (a) and (b) respectively.

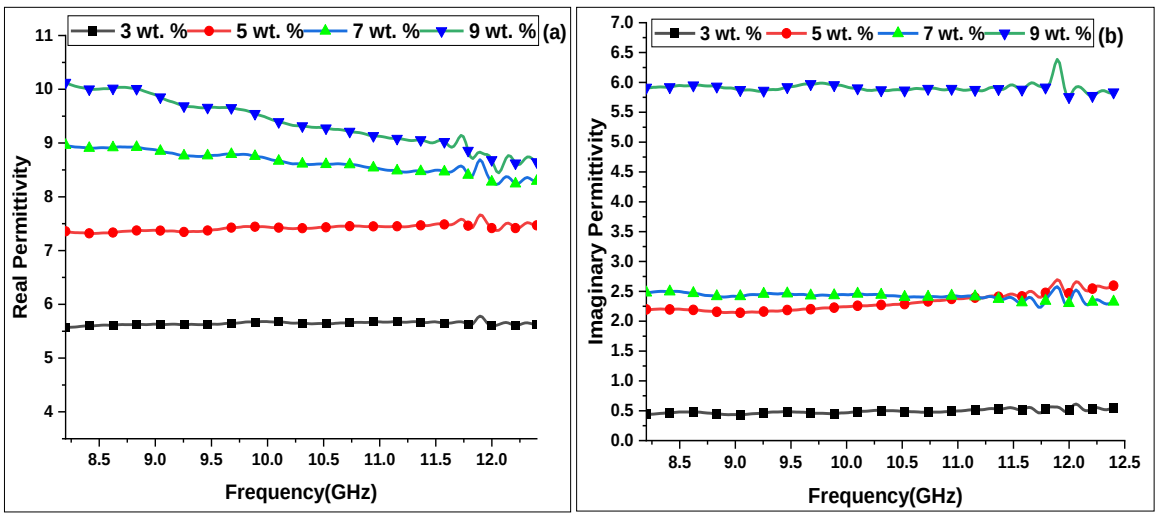

Figure 9. Relative Complex Permittivity of R-CNFs/Epoxy Composite (a) Real and (b) Imaginary Permittivity

Figure 9 (a) shown that, increasing the loading percentage of R-CNFs in the composites, the values of the real part of permittivity (ε′) is increased. The real part (ε′) of relative complex permittivity increase from ~5.7 to 7.34 for the samples with increased R-CNFs loadings from 3 to 5 wt. %. Further increasing R-CNFs loading amount in the epoxy composites, ε′ gradually increased to about 10.10for 9 wt. % R-CNFs in the composite. Figure 9. (b) shows the imaginary part (ε″) of relative complex permittivity of the R-CNFs /epoxy composite samples. Increasing percentage of R-CNFs from 3 to 5 wt. % in the composite samples, the values of ε″ increase from

about 0.49 to about 2.19, and did not show much frequency dependence in the measured range (8.2 –2.4 GHz). However, for the composite samples with R-CNFs amount 9 wt. %, the values of ε″ increase to 5.91 and also show frequency dependence in the region from 8.2 to 12.4 GHz.

The relative complex permeability (μ) is a measure for microwave absorption properties of the material from magnetic interactions. As CNFs is dielectric material, the real part (μ') and imaginary part (μ") of complex permeability of R-CNFs are reasonably thought to be 1 and 0, respectively. Figure 10. (a) shows the real part of permeability (μ′) and figure 10. (b) shows the imaginary part of permeability (μ″) of R-CNFs/Epoxy composite. The epoxy composite of R-CNFs that shows slight enhancement of μ' and μ" values observed at 7 and 9 wt. % of R-CNFs, it might be related to the variation of trace amount of mineral and magnetic materials present in plant source. The real part of permeability (μ′) in the range from 1.01 to 1.11, and the imaginary part of permeability μ″ remained at the value of ~0.06.

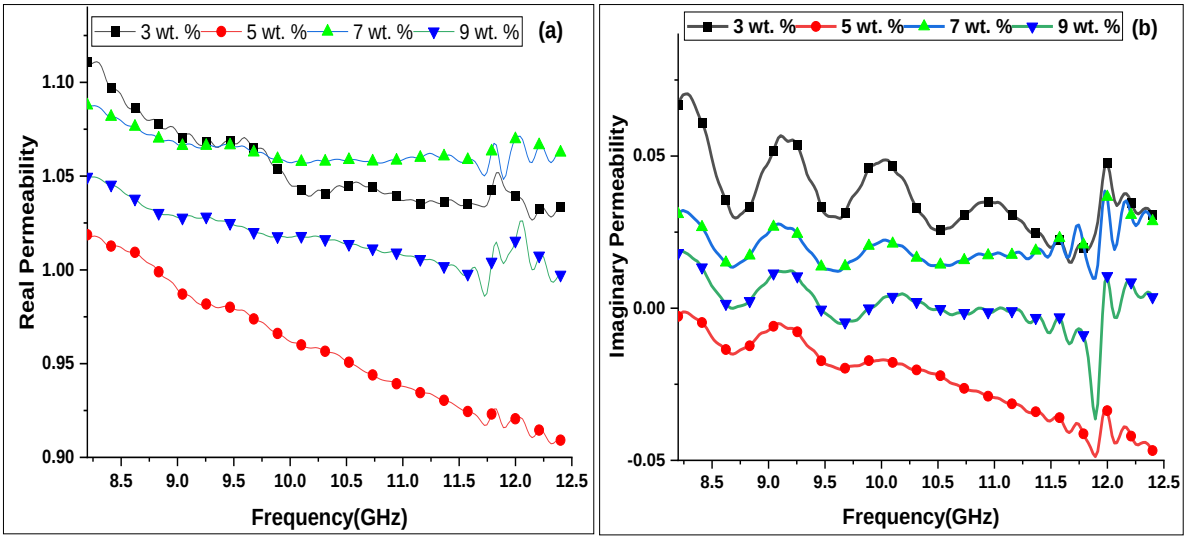

Figure 10. Relative Complex Permeability of R-CNFs/Epoxy Composite
(a) Real and (b) Imaginary Permeability

In order to further understand the loading of R-CNFs/epoxy composite on the electromagnetic properties, the dielectric loss (tan δε) was calculated as a function of frequency by following equation [29, 30].

$$\tan \delta\varepsilon = \frac{\varepsilon''}{\varepsilon'}$$

The dielectric loss is a critical factor to evaluate the electromagnetic performance of materials. The dielectric loss was investigated, and the results are shown in Figure 11. The higher tan δε value, more electromagnetic energy can be transformed into other forms of energy, mainly thermal energy. The R-CNFs/Epoxy composite shows enhanced in the dielectric tangent loss with increasing R-CNFs content.The dielectric loss (tan δε) value of 9 wt. % R-CNFs/epoxy composite are around (0.59) that implies the strong dielectric loss capacity together with high impedance matching. Whereas, the dielectric loss value of 3-7 wt. % R-CNFs/epoxy composite is approx. 0.07-0.31 which is smaller value than required (0.5), which could give poor impedance matching characteristic and unfavourable for microwave absorption.

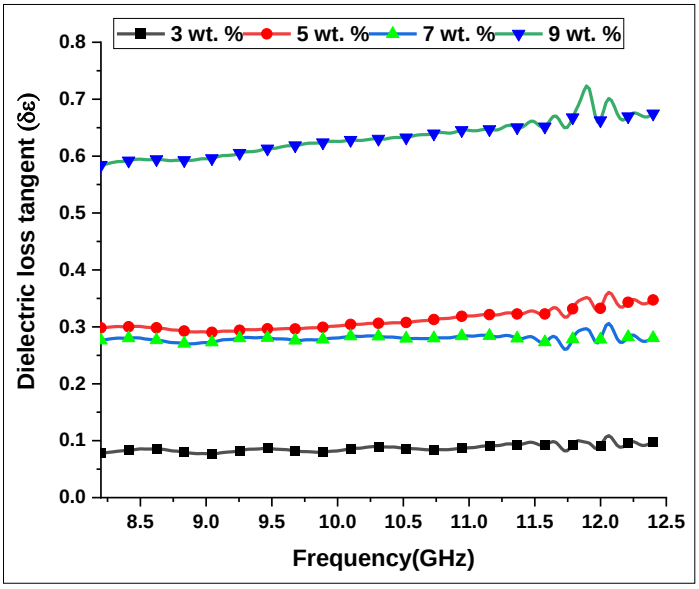

Figure 11. Dielectric loss tangent of R-CNFs/Epoxy Composite

According to Debye theory, the complex permittivity could be deduced as follows [23, 31]:

$$\varepsilon' - \left(\frac{\varepsilon_s + \varepsilon_\infty}{2}\right)^2 + (\varepsilon'')^2 = \left(\frac{\varepsilon_0 - \varepsilon_\infty}{2}\right)^2$$

Where,

ε' and ε'' are the real part and imaginary part of permittivity, respectively.

ε_s is the static permittivity,

ε_∞ is the relative dielectric permittivity at the high frequency limit, and

ε_0 is the dielectric constant in vacuum.

It could be concluded from the equation that the plot of ε'' versus ε' was a semicircle, which was known as Cole-Cole semicircle. Each semicircle corresponded to a Debye relaxation process. Figure 12 was the plot of ε' versus ε" of R-CNFs/epoxy composite. Figure 12. (a) and (b) shows the totally disordered curve of Cole-Cole plot, that implying no dielectric relaxation process in R-CNFs/epoxy composite as well as no semicircles could be observed for R-CNFs in the plots for 3 and 5 wt. %, respectively, which could prove the absent of Debye relaxation processes [32]. Whereas, figure 12. (c) and (d) shows several semicircles could be observed, for 7 and 9 wt. % R-CNFs/epoxy composite, respectively prove the multiple Debye relaxation processes and since straight line at the end of curve prove the strong conductive loss capacity for R-CNFs /epoxy composite.

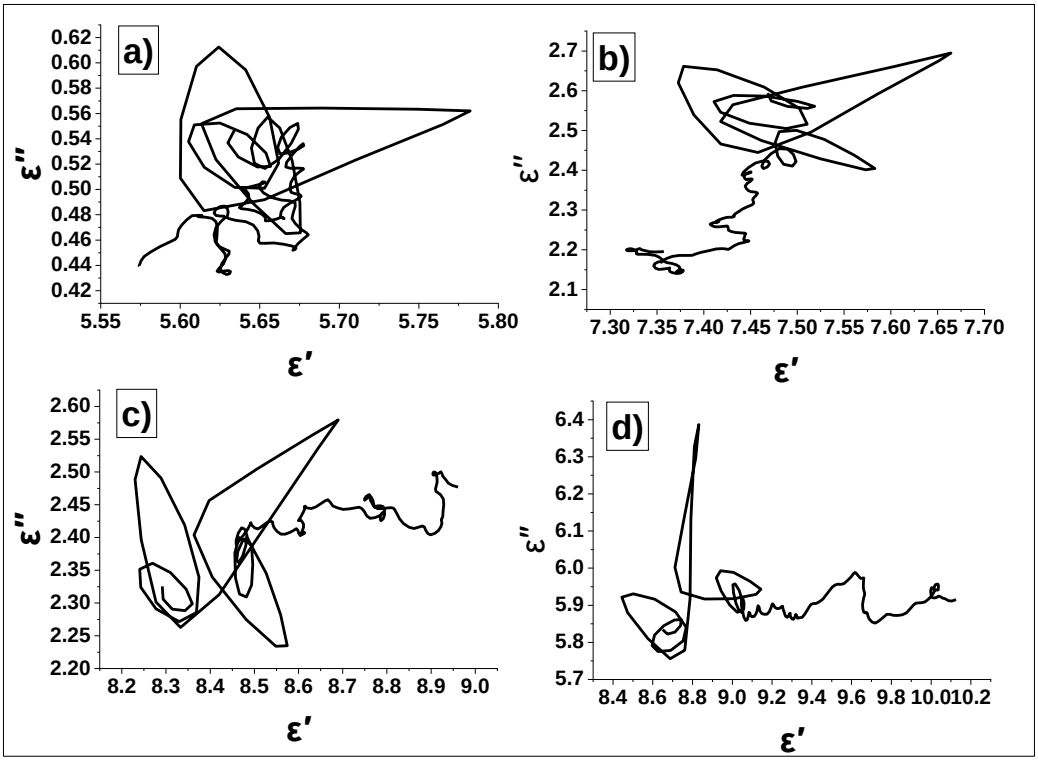

Figure 12. The Cole-Cole semicircle (ε' vs. ε") of R-CNFs/ epoxy composite a) 3, b) 5, c) 7 and d) 9 wt. % loading of R-CNFs

Attenuation constant (α) shows the ability of microwave entering into the absorbing materials [2, 20], hence attenuation ability also determines. Figure 13 shows the attenuation constant for R-CNFs/ Epoxy Composites with 2.5 mm thickness. In the X band range, the attenuation constant was increased with increasing R-CNFs concentration. From all 4 samples mentioned above, 9 wt. % R-CNFs/ Epoxy shows the highest attenuation constant, which leads to better performance of R_L.

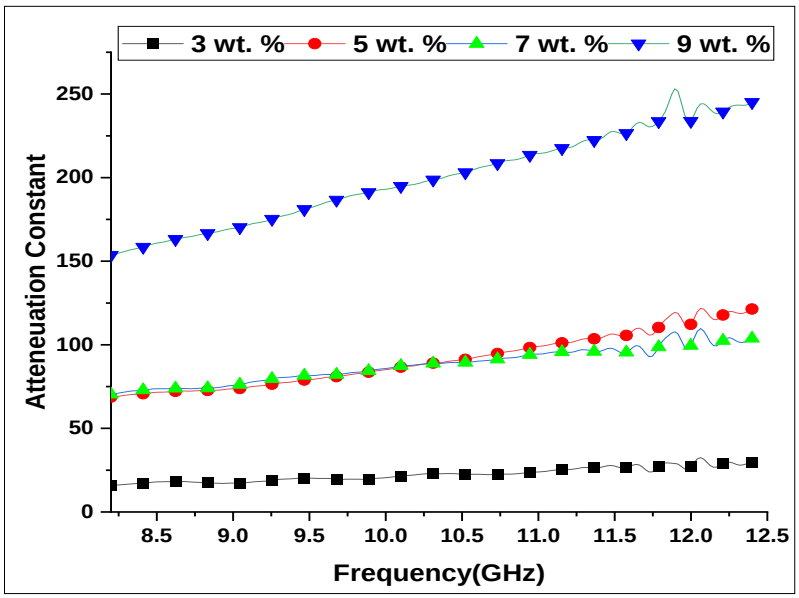

Figure 13. Attenuation Constant of R-CNFs/Epoxy Composite with Different wt. %

The microwave absorption performance of R-CNFs/Epoxy composite at 2.5 mm thickness and composition at 3, 5, 7 and 9 wt. % of R-CNFs are demonstrated in figure 14. The R_L value less than -10 dB indicated that the

microwave absorptivity of R-CNFs exceeded 90%, and the absorptivity reached 99%. [32, 33] It was apparent that the maximum R_L was obtained with 7 wt. % of R-CNFs/Epoxy composite i.e., -15.06 dB at 10.24 GHz with the thickness of 2.5 mm, illustrating that the microwave was almost 99% absorbed. The effective absorption bandwidth was 8.20-10.56 GHz.

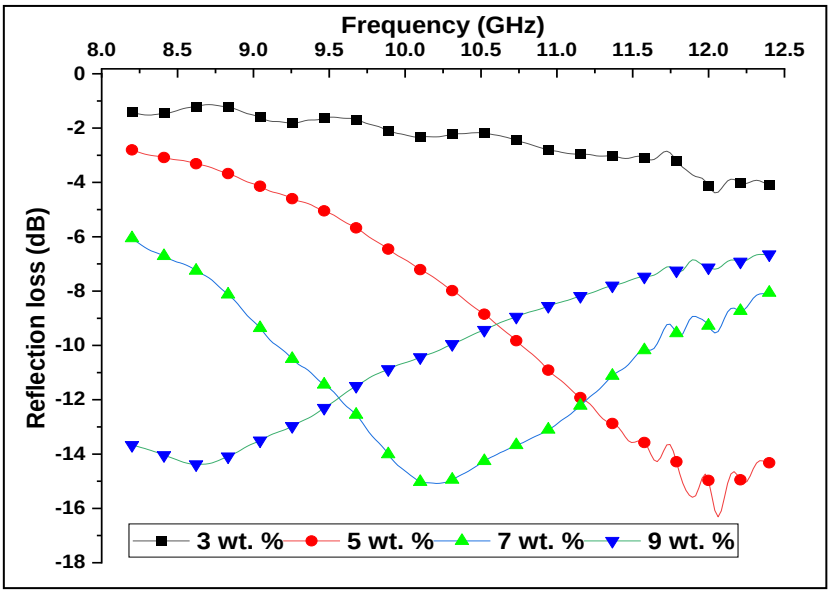

Figure 14. Reflection loss Vs Frequency Plot of R-CNFs/Epoxy Composite with Different wt. %

The above 4 mm thickness, the composite materials are not suitable for MA application. The simulation evidenced that for any filler concentration there is a maximum absorption that appears at different frequencies depending on sample thickness[34]. According to Reflection loss equation, the thickness (d) of absorbers can also affect the reflection loss; thus, the relationship between the thickness and the reflection loss of R-CNFs/ epoxy composite is investigated and shown in Figure 15.

It was observed that the frequency at which the maximum MA value appears, that shifts toward lower frequencies with increasing sample thickness. Moreover, results also indicated that, the maximum absorption peak moves to lower frequencies as the R-CNFs (conductive filler) content decrease.

Figure 15 (a), shows that the R-CNFs/Epoxy composite having 3 wt. % R-CNFs exhibit lower microwave absorption performance and that cannot reach -10 dB (90%) R_L with the thickness ranging 2-4 mm**.** The electromagnetic wave absorption performance of 5, 7 and 9 wt. % R-CNFs/Epoxy composite was found to be increasing and showing -10dB R_L. The R_L value for 5 wt. % of R-CNFs is -13.71 dB at 10.12 GHz have a thickness 2.9 mm as shown in figure 15 (b). The effective bandwidth for R_L($R_L \leq$-10 dB) is found to be 9.19-11.32 GHz for 5 wt. %.Similarly, R_L value can reach with 7 wt. % of R-CNFs is -14.48 dB at 9.10 GHz have a thickness 2.7 mm as shown in figure 15 (c). The effective bandwidth for R_L($R_L \leq$-10 dB) is found to be 8.29-10.56 GHz for 7 wt. %.The optimal R_L value can reach with 9 wt. % of R-CNFs is -13.75 dB at 9.78 GHz have a thickness 2.4 mm as shown in figure 15 (d). The effective bandwidth for R_L($R_L \leq$-10 dB) is found to be 8.41-11.88 GHz for 9 wt. %.

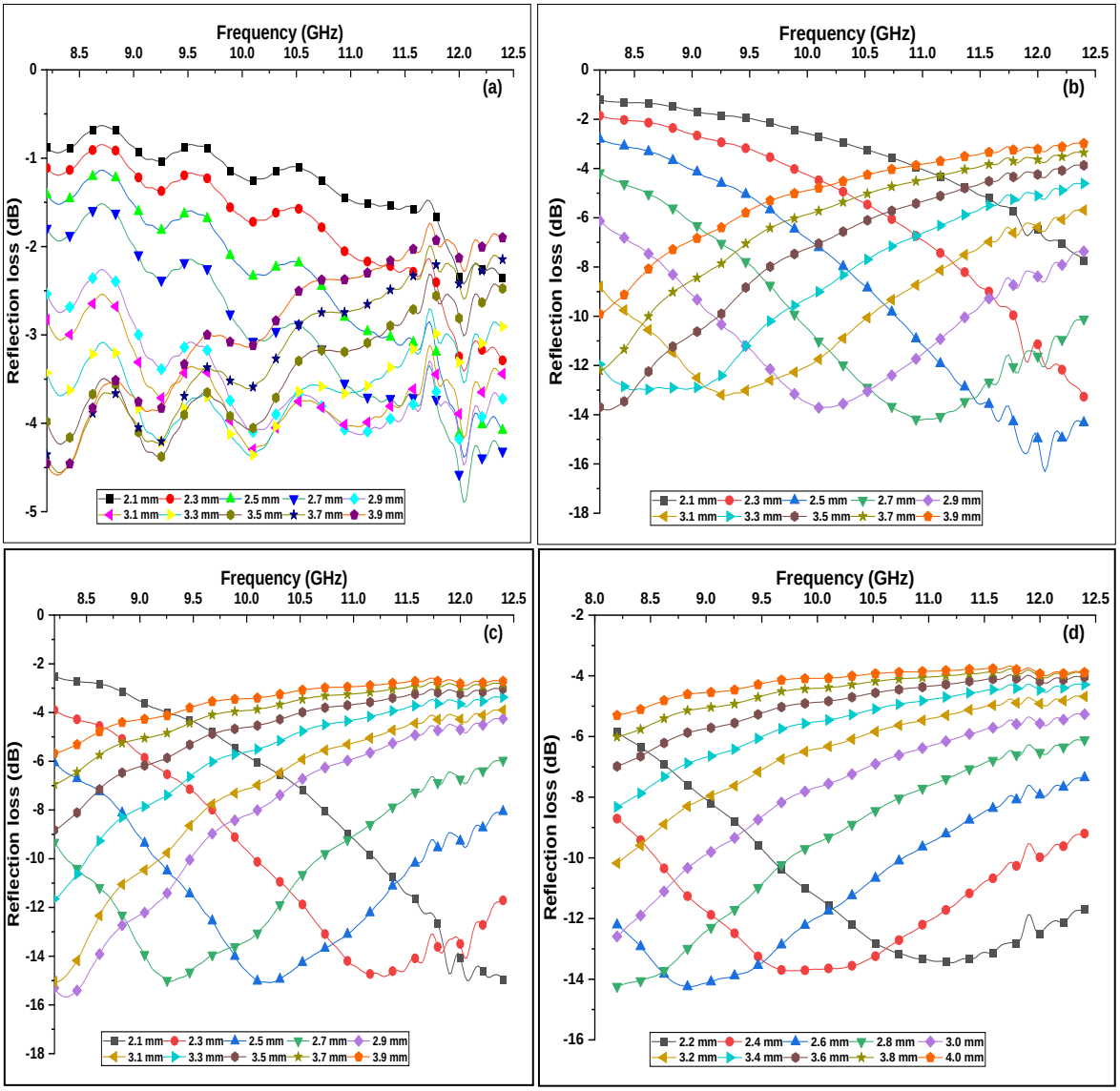

Figure 15. Reflection loss Vs Frequency Plot of R-CNFs/Epoxy Composite with Different Thickness of (a) 3 wt.%, (b) 5 wt.%, (c) 7 wt.%, (d) 9 wt.%

5. Conclusion

The novel one-dimensional CNFs has been synthesized by CVD furnace by thermal pyrolysis method using stem of rice crop as carbon source. R-CNFs, using KOH treated stem of rice crop were synthesized at 900ºC and annulled for 120 min at Hydrogen gas atmosphere. R-CNFs are tubular and having porous structure. The diameter in the range of 100-280 nm and 100-800 nm respectively. The average tube diameter and length of the R-CNFs are 161 nm and 587 nm respectively.

The effects of R-CNFs loading on the microwave adsorption performance have been investigated. The study shows that with the increasing weight percentage of R-CNFs/Epoxy composite the relative complex permittivity was increases were as with the increasing frequency (8.2-12.4GHz) the relative complex permittivity was decreases. The epoxy composite of R-CNFs shows the -10 dB R_L for 7 and 9 wt. % of R-CNFs.

The study also shows that with increasing wt. % of R-CNFs the R_L was increases. In order to achieve broad bandwidth and high R_L wt. % and thickness of R-CNFs/ polymers composite was optimized. The matching thickness and R_L characteristics in the X-band of R-CNFs/Epoxy Composite are shown in table 1 as well as in

figure 16. Results shows the relatively good microwave absorbing properties of epoxy composite at higher concentration i.e., 9 et. % of R-CNFs.

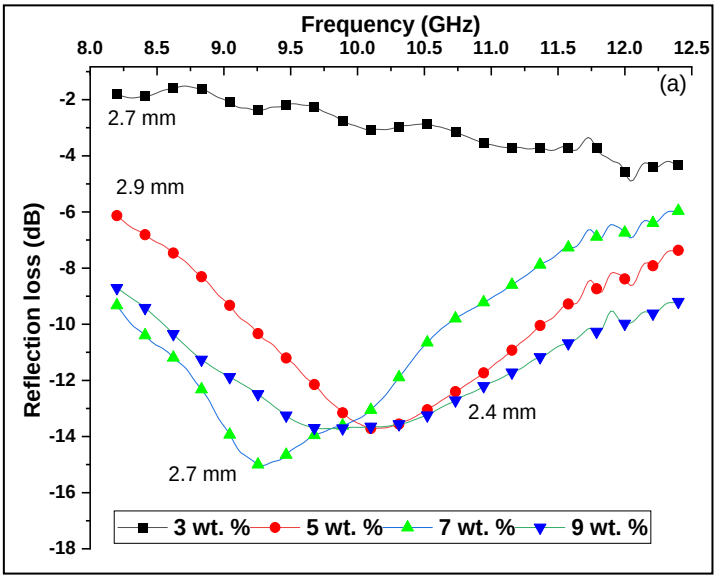

Figure 16. Matching Thickness and Reflection lossCharacteristics of R-CNFs/Epoxy Composite.

Table 1. Matching Thickness and Reflection loss Characteristics of R-CNFs/Epoxy Composite.

Polymer	R-CNFs Wt. %	Thickness (mm)	R_L (max) (dB)	Frequency (GHz)	Absorption bandwidth (GHz)	
					(R_L:10 dB)	(R_L:20 dB)
Epoxy Composite	5	2.9	-13.71	10.12	9.19-11.32	--
	7	2.7	-14.48	9.10	8.29-10.59	--
	9	2.4	-13.75	9.78	8.41-11.88	--

Based on above discussion of the present work we concluded that, the CNFs obtained from stem of rice crop shows maximum microwave absorption capacity (-13.75 dB at 9.78) with wide bandwidth of 8.41-11.88 GHz. The R-CNFs is light weight, economical, eco-friendly, having large surface area, which are suitable for application in microwave absorbing materials as well as reduction of electromagnetic radiation pollution.

6. Acknowledgments

Authors are grateful to Management, Director Dr. Naresh Chandra, Principal, Dr, Avinash Patil and Head, Department of Chemistry of B. K. Birla College Kalyan for their motivation and support for experimental work.

Refrences

[1] Singh D, Kumar A, Meena S, et al. Analysis of frequency selective surfaces for radar absorbing materials. *Progress In Electromagnetics Research B* 2012; 297–314.

[2] Jaybhaye S, Kshirsagar D, Debdatta R, et al. Microwave absorption performance of MWCNTS derived from plant based oil. *Mater Today Proc*. Epub ahead of print 2023. DOI: https://doi.org/10.1016/j.matpr.2023.01.016.

[3] Komarov V V. A review of radio frequency and microwave sustainability-oriented technologies. *Sustainable Materials and Technologies*; 28. Epub ahead of print 1 July 2021. DOI: 10.1016/j.susmat.2020.e00234.

[4] Ma Y, Zhou Y, Sun Y, et al. Tunable magnetic properties of Fe3O4/rGO/PANI nanocomposites for enhancing microwave absorption performance. *J Alloys Compd* 2019; 796: 120–130.

[5] Xu Z, Zhou H, Tan S, et al. Ultralight super-hydrophobic carbon aerogels based on cellulose nanofibers/poly(vinyl alcohol)/graphene oxide (CNFs/PVA/GO) for highly effective oil-water separation. *Beilstein Journal of Nanotechnology* 2018; 9: 508–519.

[6] Li J, Hietala S, Tian X. BaTiO3 supercages: Unusual oriented nanoparticle aggregation and continuous ordering transition in morphology. *ACS Nano* 2015; 9: 496–502.

[7] Gaud B, Singh A, Jaybhaye S. Synthesis of Carbon Nano fibre from Organic solid waste. *International Conference on Materials and Environmental Science (ICMES-2018)* 2018; 311–314.

[8] Gaud B, Singh A, Jaybhaye S. Synthesis of Carbon Fibers and Its Surface Area Mesurments. *Int J Sci Res Sci Eng Technol* 2018; 5: 10–14.

[9] Sharon M, Sharon M. Carbon nanomaterials and their synthesis from plant-derived precursors. *Synthesis and Reactivity in Inorganic, Metal-Organic and Nano-Metal Chemistry* 2006; 36: 265–279.

[10] Miah G, Rafii MY, Ismail MR, et al. Blast resistance in rice: a review of conventional breeding to molecular approaches. *Mol Biol Rep* 2012; 40: 2369–2388.

[11] Cother EJ, Noble DH, van de Ven RJ, et al. Bacterial pathogens of rice in the Kingdom of Cambodia and description of a new pathogen causing a serious sheath rot disease. *Plant Pathol* 2010; 59: 944–953.

[12] Singh A, Jaybhaye S, Dubey, Harish Kumar SK, et al. Effluent Treatment by Multi Walled Carbon Nano Tubes. *National Conference on 'Advanced Analytical Tools for Materials Characterization' (AATMC-2018)* 2018; 5: 197–200.

[13] Brijesh G, Amrita S, Sandesh J. *Optimization of Synthesis Parameters for Multiwall Carbon Nano Tubes and its Electrical Application*, www.ijcrt.org (2023).

[14] Liu X, Wang T, Kong J, et al. Effect of rice husk powder as a binder on mechanical and thermal properties of ZrO2 hollow-fiber refractory bricks. *Ceram Int* 2021; 47: 8685–8691.

[15] Liu Q, Yin C, Li X, et al. Lodging resistance of rice plants studied from the perspective of culm mechanical properties, carbon framework, free volume, and chemical composition. *Sci Rep*; 12. Epub ahead of print 1 December 2022. DOI: 10.1038/s41598-022-24714-4.

[16] Liu J, Wang Z, Guo X. Stem Characteristic Associated with Lodging Resistance of Rice Changes with Varied Alternating Drought and Flooding Stress. *Agronomy*; 12. Epub ahead of print 1 December 2022. DOI: 10.3390/agronomy12123070.

[17] Elsayed MA, Zalat OA. Factor Affecting Microwave Assisted Preparation of Activated Carbon from Local Raw Materials. *International Letters of Chemistry, Physics and Astronomy* 2015; 47: 15–23.

[18] Ojedokun AT, Bello OS. Liquid phase adsorption of Congo red dye on functionalized corn cobs. *J Dispers Sci Technol* 2017; 38: 1285–1294.

[19] Szybowicz M, Nowicka AB, Dychalska A. *Characterization of carbon nanomaterials by raman spectroscopy*. Elsevier Ltd. Epub ahead of print 2018. DOI: 10.1016/B978-0-08-101973-3.00001-8.

[20] Brijesh G, Amrita S, Sandesh J, et al. Synthesis of Carbon Nano Fiber from Organic Waste and Activation of its Surface Area. *International Journal of Physics Research and Applications* 2019; 2: 056–059.

[21] Yu K, Wang J, Song K, et al. Hydrothermal synthesis of cellulose-derived carbon nanospheres from corn straw as anode materials for lithium ion batteries. *Nanomaterials*; 9. Epub ahead of print 2019. DOI: 10.3390/nano9010093.

[22] Agyemang FO, Tomboc GM, Kwofie S, et al. Electrospun carbon nanofiber-carbon nanotubes coated polyaniline composites with improved electrochemical properties for supercapacitors. *Electrochim Acta* 2018; 259: 1110–1119.

[23] Long A, Zhao P, Liao L, et al. Sustainable Kapok Fiber-Derived Carbon Microtube as Broadband Microwave Absorbing Material. *Materials*; 15. Epub ahead of print 1 July 2022. DOI: 10.3390/ma15144845.

[24] Sun J, Wang W, Yue Q. Review on microwave-matter interaction fundamentals and efficient microwave-associated heating strategies. *Materials*; 9. Epub ahead of print 2016. DOI: 10.3390/ma9040231.

[25] Huang Z, Zhou W, Kang W, et al. Dielectric and microwave-absorption properties of the partially carbonized PAN cloth/epoxy-silicone composites. *Compos B Eng* 2012; 43: 2980–2984.

[26] Chauhan DS, Mazumder MAJ, Quraishi MA, et al. Microwave-assisted synthesis of a new Piperonal-Chitosan Schiff base as a bio-inspired corrosion inhibitor for oil-well acidizing. *Int J Biol Macromol* 2020; 158: 231–243.

[27] Xiaosi Qi,† Yu Deng,† Wei Zhong,*,† Yi Yang,† Chuan Qin,† Chaktong Au,* and YD. Controllable and Large-Scale Synthesis of Carbon Nanofibers, Bamboo-Like Nanotubes, and Chains of Nanospheres over Fe / SnO 2 and Their Microwave-Absorption Properties. *Society* 2010; 808–814.

[28] Sun Q, Zhang X, Liu R, et al. Tuning the Dielectric and Microwaves Absorption Properties of N-Doped Carbon Nanotubes by Boron Insertion. *Nanomaterials* 2021; 11: 1164.

[29] Zeng X, Cheng X, Yu R, et al. Electromagnetic microwave absorption theory and recent achievements in microwave absorbers. *Carbon N Y* 2020; 168: 606–623.

[30] Pattanayak SS, Laskar SH, Sahoo S. Microwave absorption performance enhancement of corn husk-based microwave absorber. *Journal of Materials Science: Materials in Electronics* 2021; 32: 1150–1160.

[31] Qiu X, Wang L, Zhu H, et al. Lightweight and efficient microwave absorbing materials based on walnut shell-derived nano-porous carbon. *Nanoscale* 2017; 9: 7408–7418.

[32] Wang J, Huyan Y, Yang Z, et al. Tubular carbon nanofibers: Synthesis, characterization and applications in microwave absorption. *Carbon N Y* 2019; 152: 255–266.

[33] Wang T, Li Y, Wang L, et al. Synthesis of graphene/α-Fe2O3 composites with excellent electromagnetic wave absorption properties. *RSC Adv* 2015; 5: 60114–60120.

[34] Cui C, Du Y, Li T, et al. Synthesis of electromagnetic functionalized Fe3O4 microspheres/polyaniline composites by two-step oxidative polymerization. *Journal of Physical Chemistry B* 2012; 116: 9523–9531.